LEVEL SET BASED NONLOCAL SURFACE RESTORATION

BIN DONG, JIAN YE, STANLEY OSHER, AND IVO DINOV

Abstract. In this paper we extend nonlocal smoothing techniques for image regularization in [12] to surface regularization, with surfaces represented by level set functions. We test our algorithm on both phantom and observed surfaces, including city terrain and cortical surfaces.

1. Introduction

Variational and partial differential equations (PDEs) based image denoising models have had great success in the past twenty years (see e.g. [18, 16, 3, 25]). The goal is to remove noise (in the form of random high frequency oscillations) from an image, while keeping features, e.g. sharp edges and textures.

Recently, some of the models used for image denoising have been extended to denoising surfaces (see [5, 6, 7, 14, 22, 23]). There are mainly two ways to represent surfaces. One is using triangular meshes, the other is implicitly, usually using level set functions. The well known advantages of handling implicitly represented surfaces over triangulated surfaces are numerical simplicity and flexibility of topological changes. Topological flexibility is important and it makes possible for our algorithm to do not only denoising, but also topology corrections. In this paper we shall focus on implicitly represented surfaces. We note that Yoshizawa, Belyaev and Seidel [24] recently introduced a nonlocal averaging algorithm for denoising triangulated surfaces. Their algorithm is also related to some earlier works on semi-local similarity-based shape descriptors and applications in shape matching, retrieval, and modelling [4, 10, 11, 19, 26]. Although both our and Yoshizawa-Belyaev-Seidel's methods are based on ideas of nonlocal means introduced by Buades, Coll and Morel [1] for image denoising, our approach is different in the sense that we are handling implicit surfaces with all their advantages. Elmoataz, Lezoray and Bougleux [9] recently introduced a nonlocal discrete regularization framework, which is the discrete analogue of the continuous Euclidean nonlocal regularization functionals in [12, 13]. This method is applied for image and manifold processing using weighted graphs of the arbitrary topologies. This approach is useful for various types of images, meshes, manifolds and data represented as graphs.

Date: Submitted on October 16, 2007; revised on February 20, 2008.

2000 *Mathematics Subject Classification.* 47A52, 68U10, 92C55.

Key words and phrases. Nonlocal operator, variational methods, level set functions, surface regularization, terrain surfaces, cortical surfaces.

E-mail address: bdong@math.ucla.edu (Bin Dong), ye@math.ucla.edu (Jian Ye), sjo@math.ucla.edu (Stanley Osher), and ivo.dinov@loni.ucla.edu (Ivo Dinov).

This research is supported by NIH P20 MH65166; NGIA HM-1582-07-C-010; NSF DUE 0716055; NSF DMS-0714807; and NIH U54 RR021813, www.ccb.ucla.edu.

1.1. **Nonlocal Means.** The nonlocal means method was introduced by Buades, Coll and Morel in [1]. They suggested the following nonlocal averaging for image denoising:

$$NL(u)(x) = \frac{1}{c(x)} \int_\Omega e^{-d_a(u(x),u(y))/h^2} u(y)dy$$

where $c(x)$ is a normalization factor and

$$d_a(u(x), u(y)) = \int_\Omega G_a(t)|u(x+t) - u(x-t)|^2 dt,$$

with G_a a Gaussian with standard deviation a. This algorithm gives excellent results in image denoising (see [1, 12]). In a later work by Buades, Coll and Morel [2], they showed that the nonlocal means filter can be extended from the linear regression neighborhood filter. They also derived and analyzed the corresponding PDE to the linear regression neighborhood filter, as well as the connection between bilateral filters [21] and Perona-Malik equations [17].

1.2. **Variational Viewpoints.** In [12, 13], Gilboa and Osher put nonlocal averaging into a variational framework (an earlier variational formulation was done in [15]). In this paper, we extend their formulation to surface denoising.

In [12, 13], the following energy was used

$$J(u) := \frac{1}{4} \int_\Omega \left|\nabla_w u\right|^2 dx.$$

(This uses ideas introduced in [27].) The corresponding gradient flow of the energy $J(u)$ is the nonlocal heat equation

$$u_t = \Delta_w u := \frac{1}{2}\mathrm{div}_w(\nabla_w u) = \int_\Omega (u(y) - u(x))w(x, y)dy, \tag{1.1}$$

for $x \in \Omega$. The discrete version of (1.1) is

$$u_j^{k+1} = u_j^k + dt \sum_{l \in \mathcal{N}_j} w_{jl}(u_l^k - u_j^k), \tag{1.2}$$

where u_j denotes the value of u at grid point j with j going over all grid points in the computational domain, and $\mathcal{N}_j$ is some neighborhood of j such that $w(l, j) > 0$ for $l \in \mathcal{N}_j$. The CFL restriction for the time step dt is

$$1 \geq dt \sum_{l \in \mathcal{N}_j} w_{jl}, \quad \forall j.$$

In [12], they showed that excellent denoising results can be obtained by using some properly chosen weight w, which is related to the kernel of nonlocal means.

The following section shows how we choose the weight w and apply (1.2) to surface denoising.

2. Numerical Strategies and Discussions

Throughout this paper, all surfaces are represented by signed distance functions. To be precise, the surface S is taken as the boundary of some domain Σ. The corresponding signed distance function ϕ satisfies: $\phi(x) < 0$, for $x \in \Sigma$; $\phi > 0$, for $x \notin \Sigma$; and $|\nabla\phi| = 1$ away from its singularities. Thus we have $S = \{x : \phi(x) = 0\}$. Our strategy for surface denoising is described as follows.

Strategy:

(1) Surfaces are represented by signed distance functions ϕ.
(2) Calculations are performed on a narrow band of zero level set of ϕ, denoted as Σ_δ with δ the width of narrow band.
(3) Choice of weight $w(x,y)$ and similarity function $D(x,y)$:

$$\begin{aligned} w(x,y) &= e^{-|x-y|^2/c_1} e^{-D(x,y)/c_2}, \\ D(x,y) &= \|\phi[x]-\phi[y]\|_2^2, \quad x \in \Sigma_\delta,\ y \in N_x, \end{aligned}$$

where N_x is a neighborhood of x within Σ_δ, and $\phi[x]$ is a 3D patch of ϕ centered at x.
(4) Under discrete formulations, the iterative scheme (1.2) now reads as

$$\phi_j^{k+1} = \phi_j^k + dt \sum_{l \in \mathcal{N}_j} w_{jl}(\phi_l^k - \phi_j^k), \tag{2.1}$$

with w_{jl} calculated as given in (3), and dt chosen to be

$$dt = 1/\max_j \{\sum_{l \in \mathcal{N}_j} w_{jl}\},$$

where j goes over all grid points in Σ_δ.
(5) Stopping time $k = K$ is chosen by the user (see the remark below for more details).

Remark 1.

(1) The reason we use a narrow band calculation is not only for numerical efficiency, but also because we want to (and should) focus more on the zero level set and its neighboring level sets. The nearby level sets contain more relevant information than distant level sets.
(2) The way of choosing weight w_{jl} in (3) is, in fact, a semi-nonlocal version of the original nonlocal means in (1.2) (see [12]). The parameter c_1 controls how much one wishes to penalize distant of two grid points in the weight, while c_2 controls how much one wishes to penalize similarity of the two patches. Larger c_1 allows one make use of more remote information, while larger c_2 gives results with sharper features (but requires more iterations in general).
(3) In the definition of similarity function $D(x,y)$ in (3), we simply measure the L_2 distance of two cubical patches without doing Gaussian smoothing first. This is because the signed distance function is not very noisy, even though its zero level set is quite noisy. Hence the direct L_2 distance gives a good measurement of similarity, which saves computation time.
(4) Here we let users to determine the stopping iteration K. The reason is that for real noisy surfaces (like the cortical surfaces from MRI scans in Section 3.2), the type of noise can be arbitrary (not necessarily Gaussian noise). Hence there is no apparent way of giving a unified stopping criteria as people did for image denoising. In our experiments below, the number of iterations is around 300 for the twin-cubes and city terrain, and around 150 for the cortical surfaces. In future, we shall define a unified stopping criteria for our method.

3. Numerical Results

In this section, we present numerical results for the algorithm given in the previous section. We will first show some denoising results for some shapes corrupted with Gaussian white noise. Then we test the algorithm on some biological data generated from high resolution MRI scans. For all experiments, the width δ of the narrow band Σ_δ is chosen to be 2, i.e. Σ_δ has grid points of 5 level sets including the approximate zero level set. For each given grid point $x \in \Sigma_\delta$, N_x is chosen to have 100 grid points which are closest to x within Σ_δ. The patch $\phi[x]$, centering at x, is taken to be of size $5 \times 5 \times 5$ (whose grid points could lie outside of Σ_δ).

All biological data, i.e. cortical surfaces and MRI images, are provided by the Laboratory of Neural Imaging, Center for Computational Biology, UCLA, http://www.ccb.ucla.edu.

3.1. **Denoising: Synthesis Noise.** The noisy level set function $\tilde{\phi}$ is given by $\tilde{\phi} = \phi + \varepsilon$, with $\varepsilon \in \mathcal{N}(0, \sigma)$. We compared our approach to mean curvature based surface regularization:

$$\phi_t = |\nabla\phi| \left(\nabla \cdot \left(\frac{\nabla\phi}{|\nabla\phi|} \right) - \lambda(H(\phi) - H(\tilde{\phi})) \right),$$

with H the Heaviside function. The parameter λ is chosen manually for each example.

Figure 1 is a man made shape, where two boxes are attached together. Mean curvature smoothing gives a fair result which removes most of the noise and preserves some edge information. Our approach gives a much better result. All noise is removed and the edges are not only preserved perfectly, but also reconstructed for some regions. This is not surprising because one can regard the nonlocal smoothing as a "copy-paste" procedure. Since the noisy shape has some sharp edges uncontaminated, the algorithm then "copies" them to the regions where the edges are lost and reconstruct them almost perfectly (as one can see from (c) in Figure 1). One may notice that some corners are not recovered from the noisy data. This is because the neighborhood N_x is not global and we are not taking rotations into account, so that within N_x, no similar information (i.e. corners) can be found. We shall take rotation into account in our future work. Figure 2 shows denoising results for a cortical surface (gray matter), where our approach preserves the features (e.g. sulci) very well. Figure 3 shows denoising results for man made city terrain surface. This is actually a harder surface to denoise than the previous ones, because the "holes" on the base of the surface make it a high genus surface, i.e. the topology is changed by noise. Also, the thickness of the base is only 3 grid points, which is hard to preserve for some algorithms. For example, the mean curvature algorithm will destroy the base as one can see from (c) of Figure 3. If one uses a triangular mesh based algorithm to denoise the surface, it will be very tricky to correct the topology and reconstruct back the base. In contrast, our algorithm here did a very good job in removing noise, and in topology corrections (see (d) of Figure 3).

3.2. **Denoising: Real Noisy Data.** The cortical surface (white matter) in Figure 4 is obtained from high-resolution MRI scans. The raw data is a volumetric mask of size $181 \times 217 \times 181$ segmented from MRI scans manually, which means the segmentation is accurate; however it is very noisy. Then the mask is transformed to a signed distance function using a fast sweeping method introduced in [20].

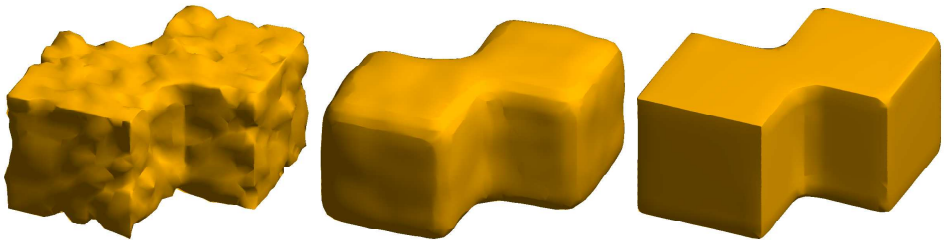

(a) (b) (c)

FIGURE 1. Figure (a) is the noisy shape; (b) is the result using mean curvature smoothing with $\lambda = 0.1$; (c) is our approach.

Cortical surfaces are much more complicated than the previous examples. First, they have very deep and narrow sulci and thin gyri. Since sulci and gyri are very important features for cortical surfaces, we want to preserve them as much as possible during regularization. In addition, the noisy cortical surfaces have lots of isolated small pieces that need to be removed. Our algorithm performed well here in removing noise and isolated pieces, while preserving sulci and gyri, as one can see from Figure 4 and Figure 5.

4. Conclusion

We have shown that our extension of nonlocal smoothing to surface regularization is very effective in removing spurious oscillations while preserving and even restoring sharp features. Furthermore, thanks to the implicit representation of surfaces, topology corrections are made by our algorithms for some of the surfaces.

References

1. A. Buades, B. Coll, and J-M. Morel. *On image denoising methods*, Multiscale Model. Simul., **4(2)** (2005), pp. 490–530.
2. A. Buades and B. Coll and J-M. Morel. *Neighborhood filters and PDE's*, Numer. Math. **105(1)** (2006), pp. 1–34.
3. M. Burger, G. Gilboa, S. Osher and J. Xu. *Nonlinear inverse scale space methods*, Commun. Math. Sci., **4(1)** (2006), pp. 179–212.
4. P. Bhat, S. Ingram and G. Turk. *Geometric texture synthesis by example*, Second Eurographics Symposium on Geometry Processing (2004).
5. U. Clarenz, U. Diewald, and M. Rumpf. *Anisotropic diffusion in surface processing*, T. Ertl, B. Hamann, and A. Varshney, editors, Proc. IEEE Vis. (2000), pp. 397–405.
6. M. Desbrun, M. Meyer, P. Schröder, and A. Barr. *Implicit fairing of irregular meshes using diffusion and curvature flow*, ACM SIGGRAPH (1999).
7. M. Desbrun, M. Meyer, P. Schröder, and A. Barr. *Anisotropic featurepreserving denoising of height fields and bivariate data*, Graphics Interface (2000).
8. M. Elsey and S. Esedoglu, *Analogue of the Total Variation Denoising Model in the Context of Geometry Processing*, CAM-Report 07–31 (2007).
9. A. Elmoataz and O. Lezoray and S. Bougleux, *Nonlocal discrete regularization on weighted graphs: a framework for image and manifold processing*, preprint (2007).
10. R. Gal and D. Cohen-Or. *Salient geometric features for partial shape matching and similarity*, under revision for ACM TOG (2005).
11. T. Gatzke, C. Grimm, M. Garland and S. Zelinka. *Curvature maps for local shape comparison*, Shape Modeling International (SMI 2005), pp. 244–256.
12. G. Gilboa and S. Osher, *Nonlocal Linear Image Regularization and Supervised Segmentation*, Multiscale Model. Simul., **6(2)**(2007), pp. 595–630.

13. G. Gilboa and S. Osher, *Nonlocal Operators with Applications to Image Processing*, CAM-Report 07–23 (2007).
14. H. Hoppe, T. DeRose, T. Duchamp, M. Halstead, H. Jin, J. McDonald, J. Schweitzer, and W. Stuetzle. *Piecewise smooth surface reconstruction*, ACM SIGGRAPH (1994), pp. 295–302.
15. S. Kindermann, S. Osher and P. W. Jones, *Deblurring and Denoising of Images by Nonlocal Functionals*, Multiscale Model. Simul., **4(4)** (2005), pp. 1091–1115.
16. S. Osher, M. Burger, D. Goldfarb, J. Xu and W. Yin, *An iterative regularization method for total variation based image restoration*, Multiscale Model. Simul., **4** (2005), pp. 460–489.
17. P. Perona and J. Malik, *Scale space and edge detection using anisotropic diffusion*, IEEE Trans. Patt. Anal. Mach. Intell., **12** (1990), pp. 629-639.
18. L. Rudin, S. Osher and E. Fatemi. *Nonlinear total variation based noise removal algorithms*, Phys. D, **60** (1992), pp. 259–268.
19. A. Sharf, M. Alexa and D. Cohen-Or. *Context-based surface completion*, ACM Trans. Graph., **23(3)** (2004), pp. 878–887. Proceedings of ACM SIGGRAPH 2004.
20. R. Tsai, L.-T. Cheng, S. J. Osher, and H. K. Zhao. *Fast sweeping method for a class of Hamilton-Jacobi equations*, SIAM J. Numer. Analy., **41** (2003), pp. 673–694.
21. C. Tomasi and R. Manduchi, *Bilateral filtering for gray and color images*, Sixth International Conference on Computer Vision (1998), pp. 839–46.
22. T. Tasdizen, R. Whitaker, P. Burchard, and S. Osher. *Geometric surface processing via normal maps*, ACM Trans. Graph., **22** (2003), pp. 1012–1033.
23. T. Tasdizen, R. T. Whitaker, P. Burchard, and S. Osher. *Geometric surface smoothing via anisotropic diffusion of normals*, Proc. IEEE Vis. (2002), pp. 125–132.
24. S. Yoshizawa, A. Belyaev and H. P. Seidel, *Smoothing by Example: Mesh Denoising by Averaging with Similarity-based Weights*, IEEE International Conference on Shape Modeling and Applications (2006), pp. 38–44.
25. J. Xu and S. Osher, *Iterative regularizaiton and nonlinear inverse scale space applied to wavelet based denoising*, IEEE Image Proc., **16(2)** (2007), pp. 534–544.
26. S. Zelinka and M. Garland. *Similarity-based surface modelling using geodesic fans*, Second Eurographics Symposium on Geometry Processing (2004), pp. 209–218.
27. D. Zhou and B. Scholkopf, *A regularization framework for learning from graph data*, ICML workshop on Statistical Relation Learning and Its Connections to Other Fields (2004).

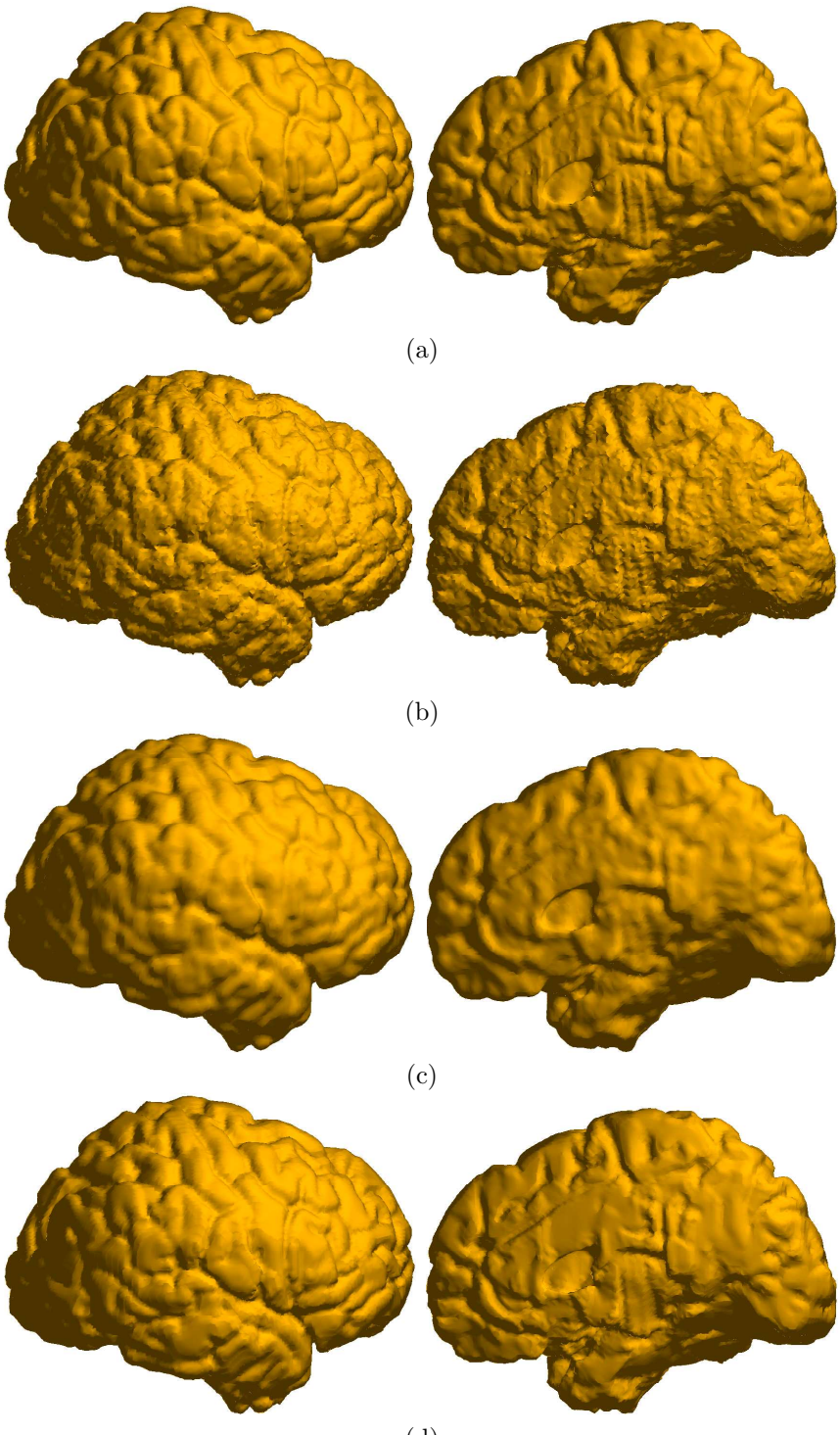

(a)

(b)

(c)

(d)

FIGURE 2. The two figures in (a), (b), (c) or (d) are the front and back views of the same cortical surface. Figure (a) is the clean gray matter; (b) is the noisy one; (c) is the denoising result from mean curvature smoothing with $\lambda = 0.001$; (d) is the result by our approach.

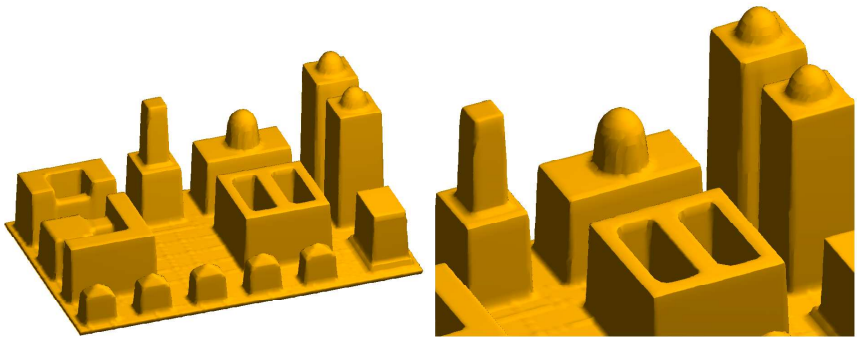

(a)

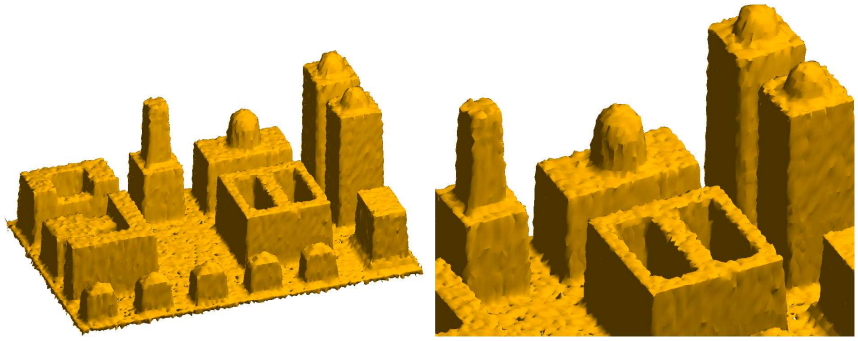

(b)

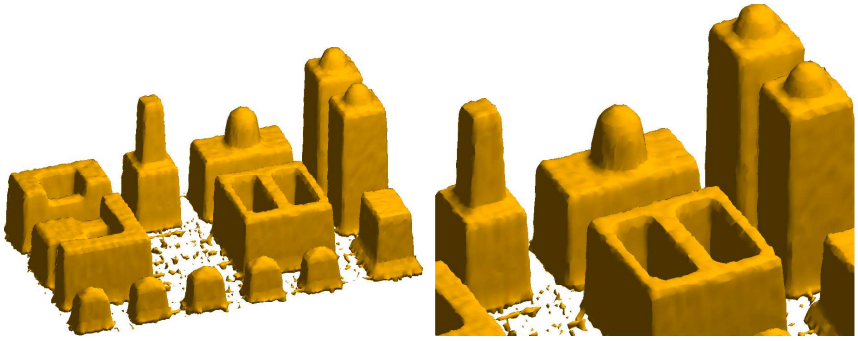

(c)

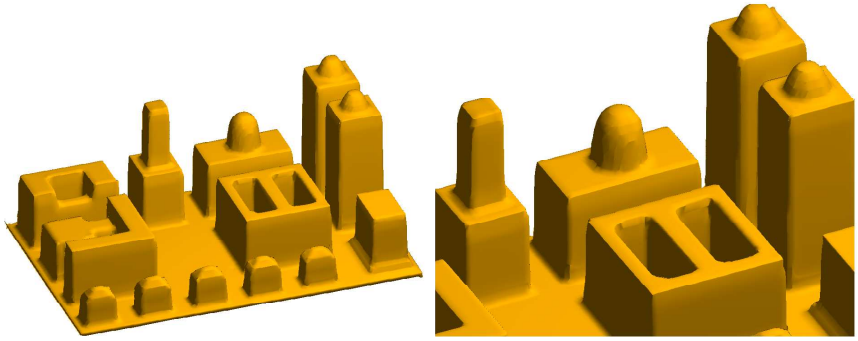

(d)

FIGURE 3. The two figures in (a), (b), (c) or (d) are the global view and a close-up of the same city terrain. Figure (a) is the clean terrain surface; (b) is the noisy one; (c) is the denoising result from mean curvature smoothing with $\lambda = 0.01$; (d) is the result by our approach.

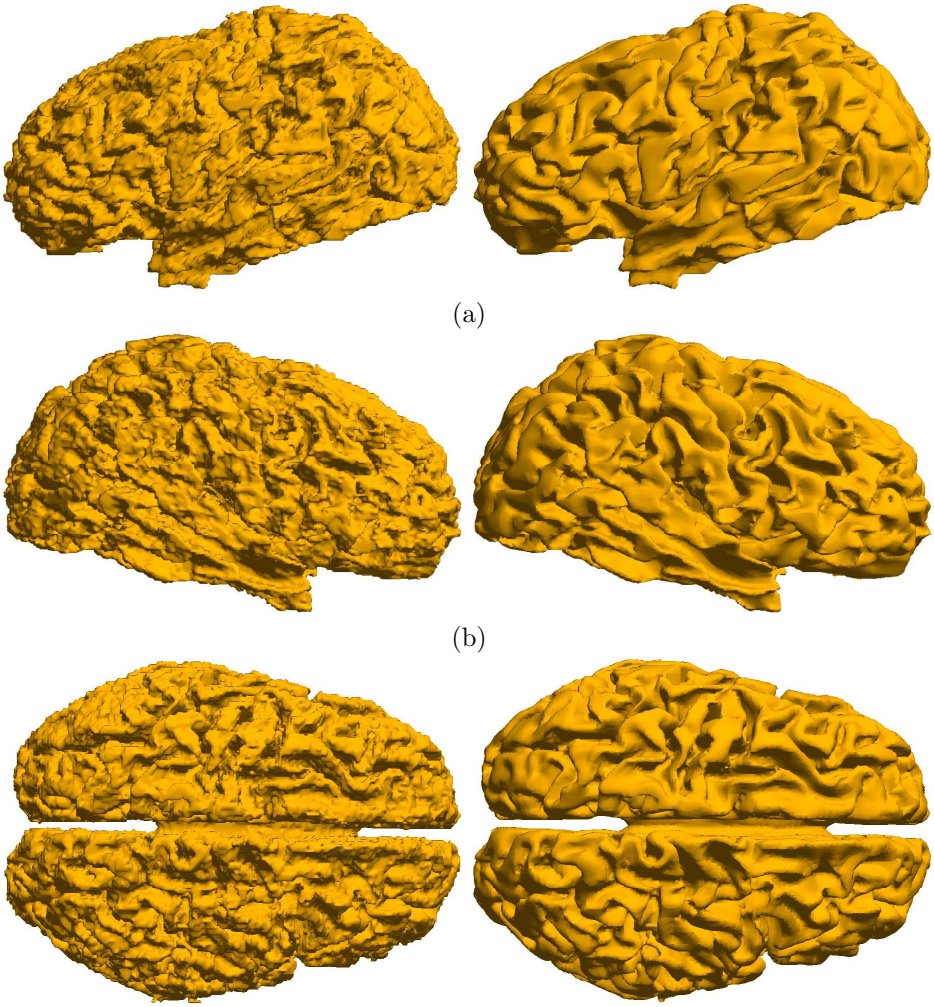

(a)

(b)

(c)

FIGURE 4. The two figures in (a), (b) and (c) are noisy (left) and regularized (right) white matter viewed from left, right and top.

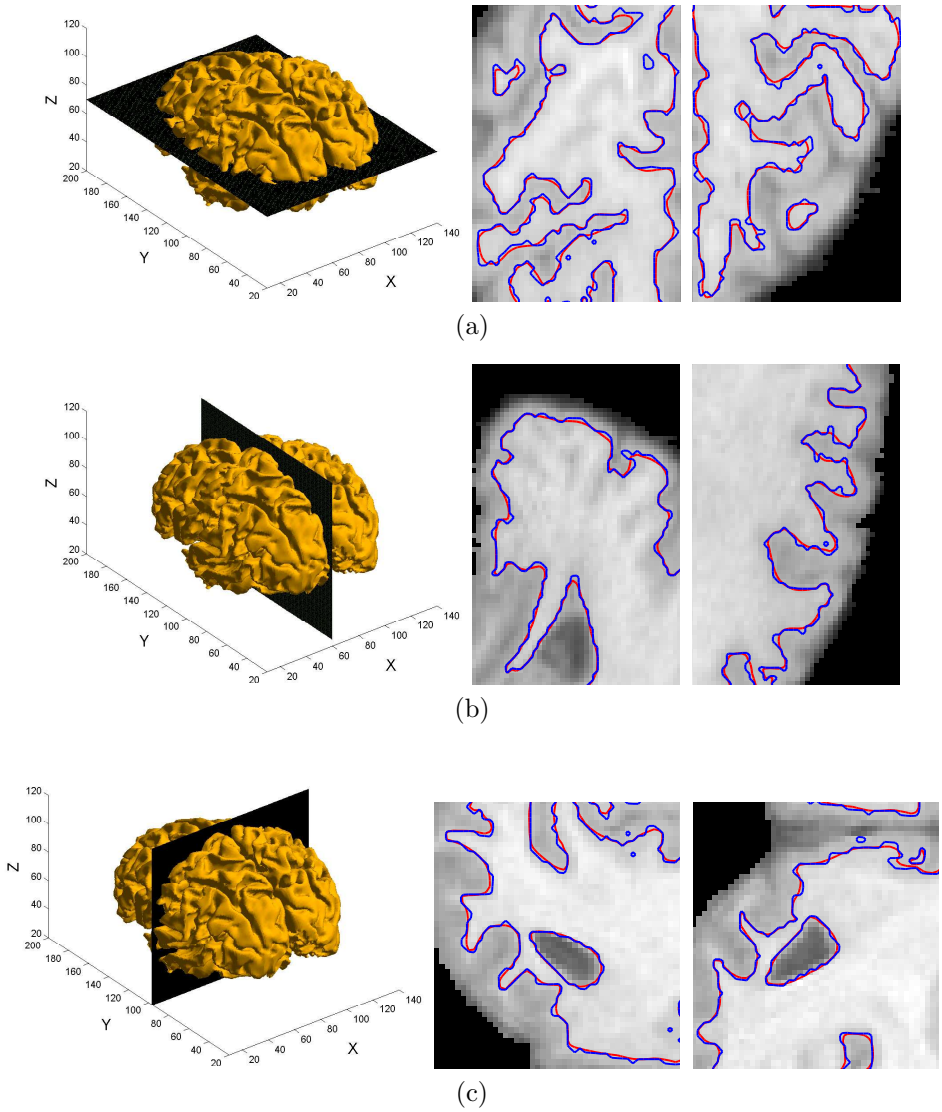

FIGURE 5. The first figure in (a), (b) and (c) illustrates which slice of the cortical surface is shown. The second and third figures in (a), (b) and (c) are the corresponding close-ups for the axial ((x, y)-slice), sagittal ((y, z)-slice) and coronal ((x, z)-slice) slices of the cortical surface and the MRI scan. Here blue curves are the original segmentation for white matter, and the red ones are regularized one.